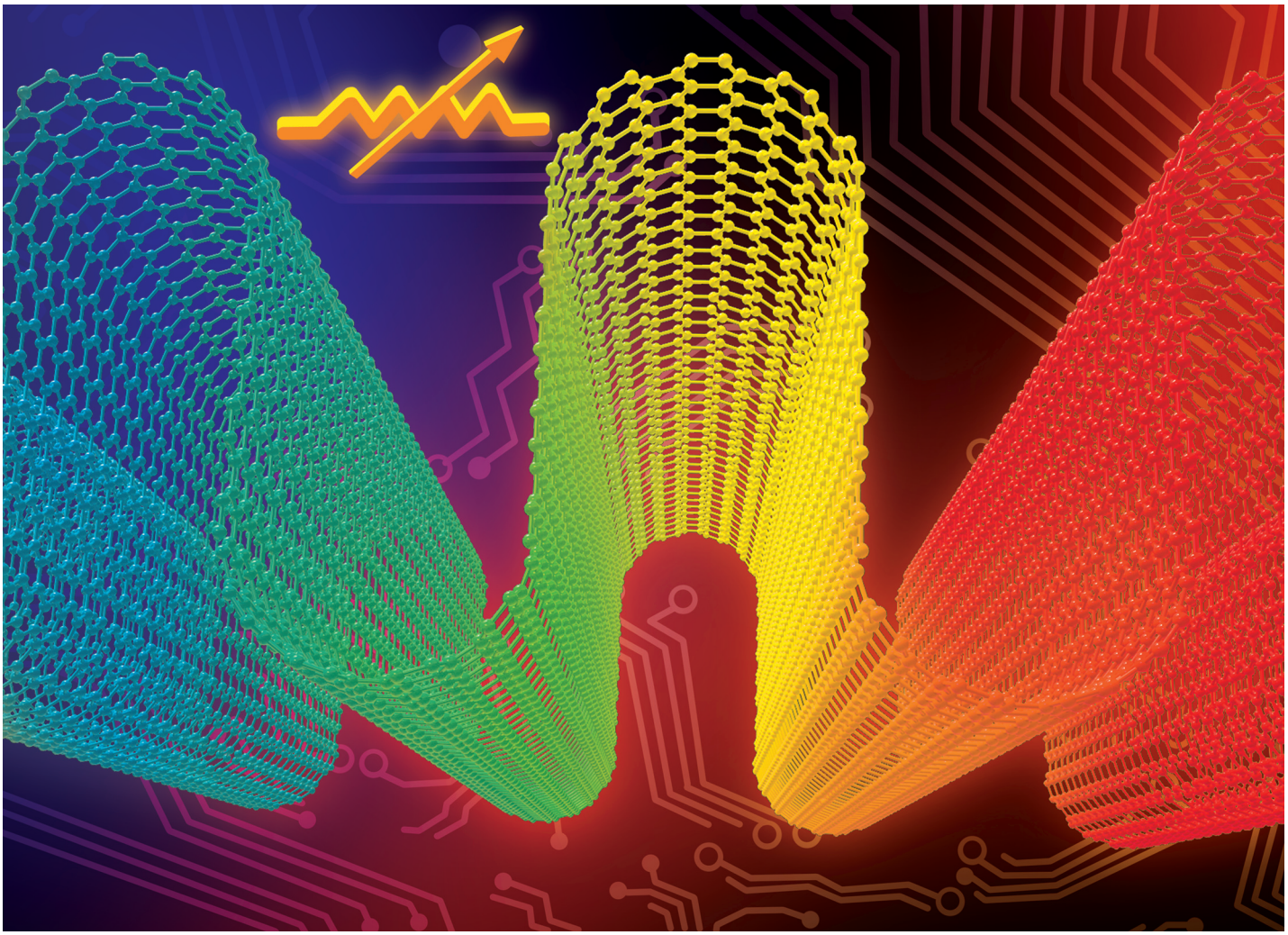

Showcasing work from the School of Energy and Power Engineering, and the School of Optical and Electronic Information, Huazhong University of Science and Technology, Wuhan, China.

Adjustable thermal resistor by reversibly folding a graphene sheet

An instantaneously adjustable thermal resistor based on folded graphene was proposed. The phonon-folding scattering effect and the dependence of thermal resistivity on the lengths of graphene were explored in theoretical analysis and simulations. The cover image demonstrates how the folded graphene, as an adjustable thermal resistor, modulates the heat flow with the temperatures denoted in colors.

As featured in:

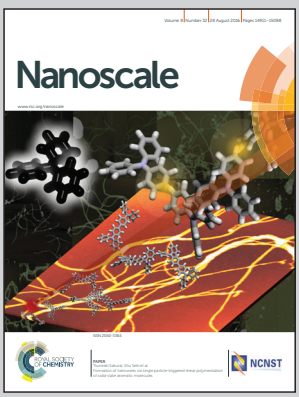

See Jianfeng Zang, Nuo Yang *et al.*, *Nanoscale*, 2016, **8**, 14943.

ROYAL SOCIETY OF CHEMISTRY

www.rsc.org/nanoscale

Registered charity number: 207890

Nanoscale

PAPER

View Article Online
View Journal | View Issue

Cite this: *Nanoscale*, 2016, **8**, 14943

Adjustable thermal resistor by reversibly folding a graphene sheet

Qichen Song,†‡[a,b] Meng An,†[a,b] Xiandong Chen,[a,b] Zhan Peng,[a,b] Jianfeng Zang*[c,d] and Nuo Yang*[a,b]

Received 9th March 2016,
Accepted 23rd June 2016

DOI: 10.1039/c6nr01992g

www.rsc.org/nanoscale

Phononic (thermal) devices such as thermal diodes, thermal transistors, thermal logic gates, and thermal memories have been studied intensively. However, tunable thermal resistors have not been demonstrated yet. Here, we propose an instantaneously adjustable thermal resistor based on folded graphene. Through theoretical analysis and molecular dynamics simulations, we study the phonon-folding scattering effect and the dependence of thermal resistivity on the length between two folds and the overall length. Furthermore, we discuss the possibility of realizing instantaneously adjustable thermal resistors in experiment. Our studies bring new insights into designing thermal resistors and understanding the thermal modulation of 2D materials by adjusting basic structure parameters.

Introduction

A detailed understanding of phonon transport enables people to manipulate heat flow at nanoscale and design phononic devices[1] based on electronic analogs, *e.g.* thermal diodes,[2] thermal transistors,[3] thermal logic gates,[4] *etc*. In electronic circuits, a variable electrical resistor (potentiometer) dynamically tuning the electric load is essential to multiple applications. However, a thermal counterpart to an instantaneously adjustable electrical resistor is rather interesting but has not yet been proposed.

The basic requirement of an adjustable electrical resistor is a simple resistance–position relationship, for example, linear characteristics, *i.e.* the electrical resistance has a linear dependence on the distance between the positions of two contacts. To develop a thermal version of the linear characteristics, it is expected that the thermal resistance of a candidate material should have a linear dependence on parameters that can be easily controlled. Recently, scientists demonstrated a great potential in tuning the transport properties of graphene simply by controlling the deformation status,[5] creating even more possibilities beyond its high electrical[6] and thermal[7] conductivities. For nanodevices based on graphene, it is viable to change the shape (*e.g.* by folding) due to their high flexibility.[8] Recent reports show that graphene nanoribbons with folds can modulate electron transport,[9,10] phonon transport[11–13] and mechanical properties.[14] Particularly, the thermal conductivity can be modulated with different numbers of folds.[15] As is well known, the size effect is an important issue in nanostructures.[12] However, most previous studies focused on graphene nanoribbons of a finite size. More recently, the reversibility of folding and unfolding large-area graphene sheets has been demonstrated in experiment,[5] making it possible to generate certain numbers of folds in an initially planar graphene or eliminate the folds from folded graphene.

Here, we propose an instantaneously adjustable thermal resistor based on the folding effects on large-area graphene. We study folded graphene with various shape parameters. Moreover, we introduce a new phonon scattering regime, named as phonon-folding scattering, which stems from this novel folded structure and explain the length-dependent behavior of the thermal resistivity of folded graphene.

Theoretical model

Experimentally, the folding and unfolding of graphene sheets can be controlled by the substrate deformation instantaneously.[5] That is, the number of folds and the degree of folding can be controlled by changing the strain of the substrate, the shear modulus of the substrate, and the adhesion

[a]*State Key Laboratory of Coal Combustion, Huazhong University of Science and Technology, Wuhan 430074, People's Republic of China. E-mail: nuo@hust.edu.cn*
[b]*Nano Interface Center for Energy (NICE), School of Energy and Power Engineering, Huazhong University of Science and Technology (HUST), Wuhan 430074, People's Republic of China*
[c]*School of Optical and Electronic Information, Huazhong University of Science and Technology, Wuhan 430074, People's Republic of China. E-mail: jfzang@hust.edu.cn*
[d]*Innovation Institute, Huazhong University of Science and Technology, Wuhan 430074, People's Republic of China*
†These authors contributed equally to this work.
‡Current address: Department of Mechanical Engineering, Massachusetts Institute of Technology, 77 Massachusetts Avenue, Cambridge, MA 02139, USA.

energy between the graphene and the substrate. A schematic of the adjustable thermal resistor based on graphene with folds is illustrated in Fig. 1(a). The device, firstly, takes the advantage of the fact that a phonon mean-free path (MFP) is relatively large in suspended graphene (100 nm–600 nm)[11,16] and phonon transport in graphene can be affected by its structure. Secondly, the resistance depends on both the number of folds and the distance between two folds due to folding. The device can achieve linear characteristics of thermal resistance and the mechanism can be explained by the following theoretical model.

It is known as the Casimir limit[17] when the phonon MFP and thermal conductivity are limited by the system size. The effective MFP[18] in a finite system, l_{eff}, is given as,

$$\frac{1}{l_{\text{eff}}} = \frac{1}{l_\infty} + \frac{2}{L}, \tag{1}$$

where l_∞ is the phonon MFP for the infinite system and L is the length of finite system. This is named as finite-size effects of phonons which are caused by boundary scattering. Between heat source and heat sink, some phonons travel ballistically across the system and the MFP of those phonons is limited by system size L. For those phonons, the average distance they travel is $L/2$. We know that there is a linear relationship between the thermal conductivity and MFP as $\kappa = C_v v_g l$. When the size effect of specific heat C_v and group velocity v_g is negligible, it can be derived from eqn (1) that the resistivity r has a linear dependence on $1/L$, as

$$r = \frac{1}{\kappa} = \frac{1}{C_v v_g}\left(\frac{1}{l_\infty} + \frac{2}{L}\right). \tag{2}$$

In nanowires or graphene ribbons, L is the longitudinal length.[19]

When there is more than one factor limiting the phonon MFP simultaneously, according to the Matthiessen rule,[20] the total scattering event can be described as follows,

$$\tau_{\text{scatt}}{}^{-1} = \sum_j \tau_{\text{scatt},j}{}^{-1}, \tag{3}$$

where τ_j is the relaxation time of the scattering process j. When eqn (3) is multiplied by $1/v_g$, then the inverse effective MFP can be written as $l_{\text{eff}}{}^{-1} = \sum_j l_j{}^{-1}$, where l_j is the characteristic length of the scattering process j.

In a folded graphene, the scattering processes include intrinsic anharmonic phonon–phonon scattering, boundary scattering, and phonon-folding scattering meaning that phonons can be scattered by folds. As shown in Fig. 1(b),

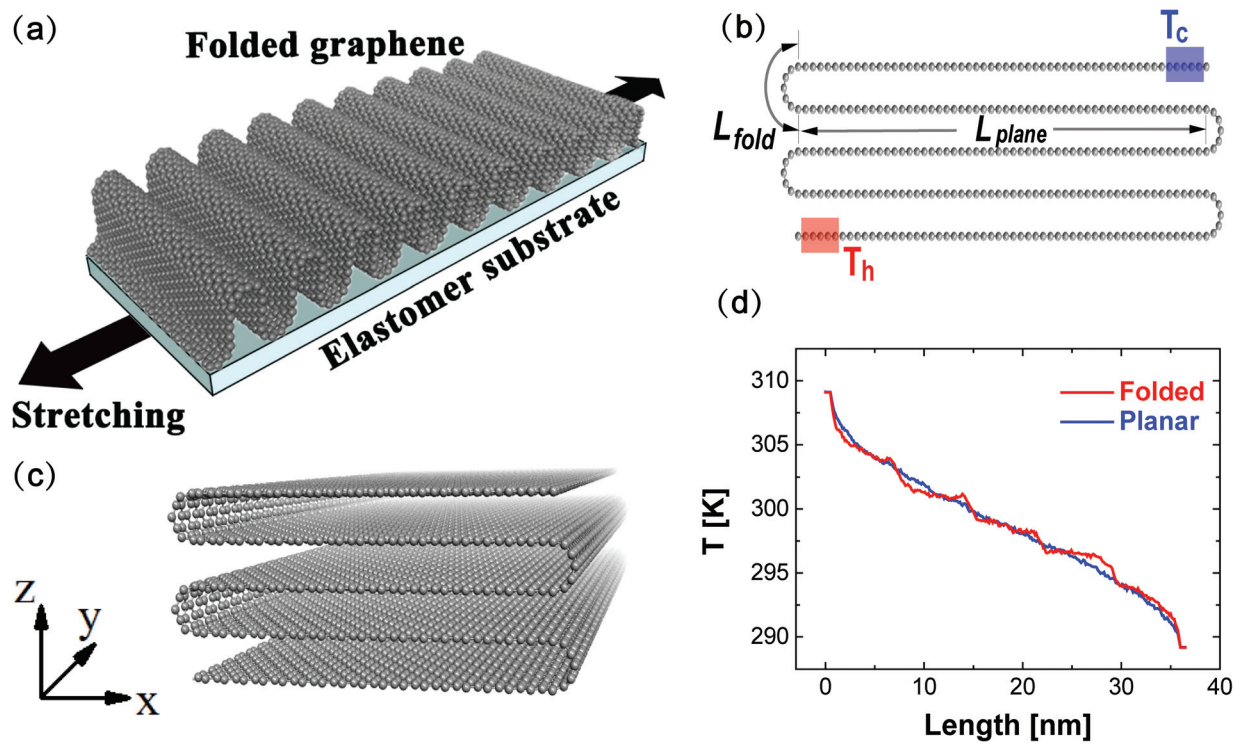

Fig. 1 (a) Schematic illustration of an instantaneously adjustable thermal resistor. (b) The side view of the structure of folded graphene before relaxation. L_{plane} and L_{fold} are 6.75 nm and 0.737 nm, respectively. The number of folds is 4 and the length L of the structure is 36.7 nm. The initial interplane distance before relaxation is 0.474 nm. The Nosé–Hoover thermostat method with high temperature (T_h) and low temperature (T_c) is applied to the bottom (red) and top (blue) graphene sheets, respectively. (c) A projection view of the structure before relaxation. The width of the system can be treated as infinitely large with periodic boundary condition along y direction. (d) The stair-step temperature distribution profiles in the structure along the longitudinal direction, compared with that in planar graphene of the same length.

between the two folds the distance is denoted by L_{plane}. Similarly to finite-size effects, the effect of phonon-folding scattering on the effective MFP has a relationship with $2/L_{plane}$. Nevertheless, the phonon-folding scattering is different from finite-size effects as some phonons can transfer through the folds without being scattered, such as some vibration modes along the y direction. So the scattering term $2/L_{plane}$ may overestimate the effect of phonon-folding scattering. Here, we add a coefficient α in front of $2/L_{plane}$ to describe the phonon-folding scattering in eqn (4). It is noted that, similar to impurity scattering, grain-boundary scattering, and isotope scattering, the phonon-folding scattering is also a disturbance to a perfect crystal. Generally, these scatterings are assumed to be independent of each other.[21,22] Therefore, the thermal resistivity of folded graphene can be described as:

$$r = \frac{1}{\kappa} = \frac{1}{C_v v_g}\left[\frac{1}{l_\infty} + 2\left(\alpha\frac{1}{L_{plane}} + \frac{1}{L}\right)\right]. \quad (4)$$

As $\kappa_\infty = C_v v_g l_\infty$, then we have

$$r = \frac{1}{\kappa} = \frac{1}{\kappa_\infty}\left[1 + 2l_\infty\left(\frac{\alpha}{L_{plane}} + \frac{1}{L}\right)\right]. \quad (5)$$

Eqn (5) is the main theoretical model and it will be proved by MD simulation results. Based on eqn (3) and (5), the ratio of relaxation time of finite-size effects to phonon-folding scattering can be calculated explicitly by the ratio of corresponding scattering terms as $\frac{\tau_{finite}}{\tau_{folding}} = \frac{L_{plane}}{\alpha L}$. When L_{plane} is finite and $L \to \infty$, the coefficient α can be fitted by $\alpha = \frac{(\eta-1)L_{plane}}{\kappa_\infty \frac{\Delta r}{\Delta(1/L)}}$, where $\eta = \frac{r_{folded}}{r_{planar}}\Big|_{\frac{1}{L}=0} = 1 + \frac{2\alpha l_\infty}{L_{plane}}$.

To design the adjustable thermal resistor, there are two possible strategies. One way is to change the length of structure and the other one is to tune its thermal resistivity directly. The former approach is hard to achieve at nanoscale since the crystal growth usually takes a long time and the size of graphene will not be changed after being fabricated. So we move our attention to the latter approach by changing thermal resistivity while keeping L invariant. Now, through modulating the distance between two folds, L_{plane}, *i.e.* changing the number of folds, n, we can adjust the thermal resistance of one single piece of graphene.

MD method

In the MD simulations, the simulation cell of the folded graphene is built as shown in Fig. 1(b and c). The length of graphene is characterized by $L = (n + 1) \times L_{plane} + n \times L_{fold}$, where n is the number of folds and L_{plane} and L_{fold} is the length of the flat part and folded part, respectively. The width of the simulation cell is set as 2.13 nm (10 atoms in each layer) for the reason that the thermal conductivity of cases with larger width is independent on width. A periodic boundary condition is applied in the y direction, and atoms in the two ends are fixed. By the Nosé–Hoover thermostat method,[23,24] the five nearest layer atoms to the fixed boundary are maintained at $T_h = (1 + \Delta) \times T$, while those nearest to the other side are at $T_c = (1 - \Delta) \times T$, where T = 300 K and Δ = 0.1. The substrate effect is included to imitate the experiment settings, where the couplings are described by the Lennard-Jones 12-6 potential.[25]

A Morse bond and a harmonic cosine potential energy including two-body and three-body potential terms[26–28] are used to describe the bonding interaction between carbon atoms. Although the force field potential is developed by fitting experimental parameters for graphite, it has been testified by the calculation of thermal conductivity of graphene[15,29] and carbon nanotubes.[26] The simulation domain is bounded with two Lennard-Jones (LJ) 12-6 potential[25] walls in the z direction that enclose atoms of the top plane and bottom plane. In all MD simulations, the Velocity–Verlet algorithm[30] is used to integrate the differential equations of motions. The time step of 0.5 fs is adopted and the total simulation time is set as 3 ns. At the very beginning of the simulation, the distance between nearest plane layers is 0.474 nm. For the first 3×10^5 steps, the positions of the both substrates are moved towards each other at a small pace ($\sim 10^{-6}$ nm per step), small enough compared with the movement of the atom at each step ($\sim 10^{-4}$ nm). Then during the rest of the evolution, the distance between the nearest plane layers is relaxed under the VDW force. After relaxation, the inter-plane distance approaches the same value, 0.350 nm, and the fold length also approaches the same value, 0.737 nm. It should be noted that the fold length decreases as the inter-plane distance decreases. Our previous work[15] observed that the thermal resistivity increases with the decreasing inter-plane distance due to the fact that compressing inter-plane distance could enhance phonon-phonon scattering. In addition, the literature shows that as the curvature for the folds increases, the thermal resistivity increases. In this work, we are looking for the regime where the resistivity depends solely on the characteristic length, thus we use the same inter-plane distance, same fold length and same curvature for all calculation cases.

The total heat flux (J_t) is recorded by the average of the input/output power of the two baths as

$$J_t = \frac{1}{N_{T_h(T_c)}}\sum_{i=1}^{N_{T_h(T_c)}}\frac{\Delta\varepsilon_i}{2\Delta t}, \quad (6)$$

where $\Delta\varepsilon$ is the energy added to/removed from each heat bath (T_h or T_c) at each step Δt. The total heat flux can be divided into the in-plane flux (J_i) and the inter-plane heat flux (J_{int}), where $J_t = J_i + J_{int.}$ In order to obtain J_i, we record the heat flux carried by the inter-plane interaction, the van der Waals (VDW) force, based on[31,32]

$$J_{int} = \sum_{i\in A,\, j\in B} J_{i\to j} = \sum_{i\in A,\, j\in B}\frac{1}{2}\left\langle \mathbf{F}_{ji}\cdot\mathbf{v}_j + \mathbf{F}_{ji}\cdot\mathbf{v}_i\right\rangle, \quad (7)$$

where $\mathbf{F}_{ji}$ is the VDW force on atom j by atom i, and A and B represent the two groups of atoms separated by a cross section

that the heat energy passes through. With that, the in-plane heat flux can be calculated by

$$J_i = J_t - J_{int}. \quad (8)$$

Here we are more interested in the in-plane phonon transport. Based on the format of Fourier's Law, the thermal conductivity can be calculated by

$$\kappa_i = -\frac{J_i}{A\nabla T}, \quad (9)$$

where J_i is the heat current along the structure, and A is the cross section area and $\nabla T = (T_h - T_c)/L$. The results presented here are the average of 12 independent simulation cases with different initial conditions and the error bar of thermal conductivity is the deviations of the 12 simulation results. In addition to the folded structures, the thermal conductivity of planar graphene is also calculated for comparison.

Results and discussion

Firstly, we studied both a planar graphene and a folded graphene of which the length L is kept the same, as 36.7 nm. The temperature distribution profiles of the folded graphene and the planar graphene are presented in Fig. 1(d). The temperature distribution in folded graphene shows a stair-step mode, which is obviously different to that of planar graphene. Each sharp change point in the temperature profile indicates a larger thermal resistivity at a fold compared to in the planes. In addition, the linear characteristic of the thermal resistivity r is simulated when we keep the overall length L to be 36.7 nm and change the distance between the two folds, L_{plane}. That is, the number of folds is changed from 1 to 7.

As shown in Fig. 2(a), it is found that r is dependent on $1/L_{plane}$ in structure. This reveals that the phonons are scattered at the folds and the MFP is restricted by the L_{plane}. More interestingly, the thermal resistivity r of folded graphene depends linearly on $1/L_{plane}$ for all calculation cases, which proves that our theoretical model of eqn (5) is valid and reasonable.

Moreover, we studied the structure of samples in which the L_{plane} values are kept the same, while the number of folds (n) and lengths (L) are different. The systems of different L values are explored in order to find the influence of the initial length of graphene before folding. As L_{plane} is fixed, the enlargement of L is solely related to the increase of the number of folds. The resistivity r with respect to $1/L$ is shown in Fig. 2(b). When the L becomes larger, r increases as $r \sim 1/L$, similar to the trend of planar graphene. This is because the decreased length L confines the phonon modes that exist in the structure. Meanwhile, the linear relationship confirms that our theoretical model of eqn (5) is valid. When we extrapolate the linear fitting curve to $1/L = 0$, it is found that the thermal resistivity of infinitely large folded graphene is 4.4 times as high as the value of graphene.

Admittedly, precisely controlling the inter-plane distance in the process of folding and unfolding of large-area graphene, especially at a nanoscale, is challenging and subject to large uncertainties. Nevertheless, the heat energy cannot be transferred *via* the weak VDW forces when the inter-plane distance reaches beyond the radius of VDW forces. Therefore, we proceeded to compare the in-plane heat flux to the total heat flux, as shown in Fig. 3. As L_{plane} decreases with the increased number of folds, the inter-plane flux is reduced since more folds leads to a smaller plane area to transport heat energy by VDW forces. Moreover, the ratio of inter-plane heat flux to the total heat flux tends toward the convergent value around 20%,

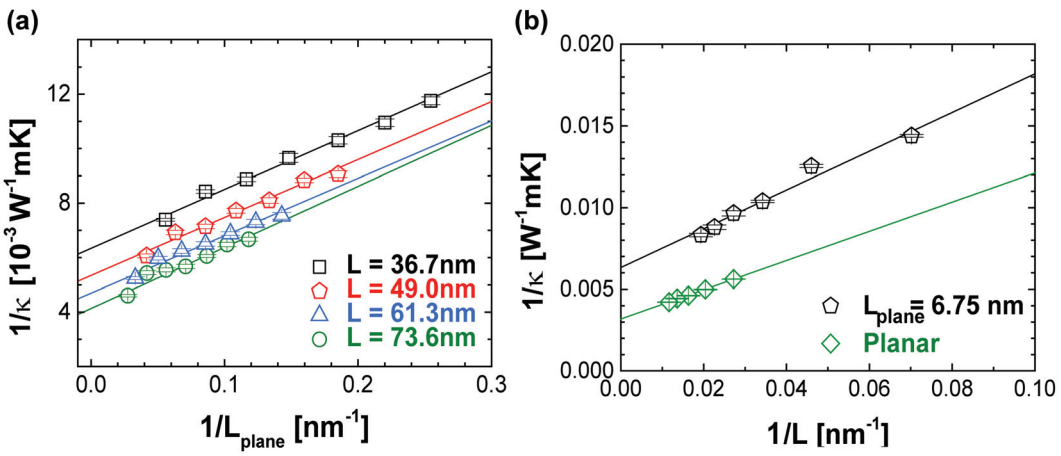

Fig. 2 (a) The size dependence of the resistivity of folded graphene on the reciprocal of length between two folds, $1/L_{plane}$. The fitting curves are based on eqn (5). Note that the length of the folded graphene is fixed, which means L_{plane} decreases as the number of folds (n) increases. The number of folds, n, ranges from 1 to 7, corresponding to seven data points in the same color from left to right. (b) The size dependence of the resistivity of planar/folded graphene on the reciprocal of length, $1/L$. The fitting curves are based on eqn (5). Note that the distance across plane between two folds, L_{plane}, is constant in folded graphene, which means that length, L, varies with number of folds (n). The number of folds, n, ranges from 2 to 7, corresponding to the six data points in black from right to left.

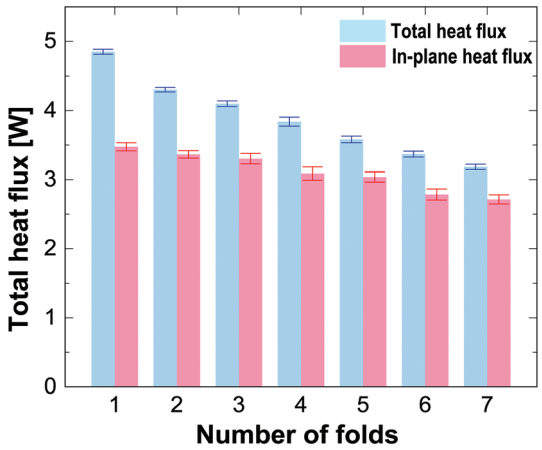

Fig. 3 Histogram of the total heat flux J_t calculated by eqn (6) and the in-plane heat flux J_i calculated by eqn (7).

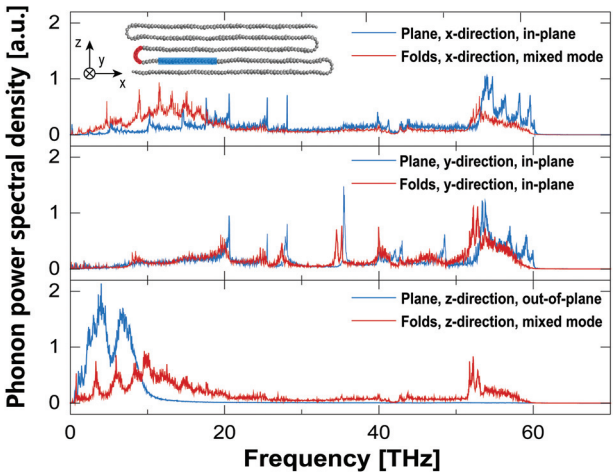

Fig. 5 The phonon power spectral density along different directions of atoms in the plane and in the fold structure, obtained by calculating the Fourier transformation of the recorded velocities along the corresponding directions of selected atoms. The details of the structure for calculation can be found in the caption of Fig. 1. Velocities of all atoms in the red area (60 atoms) are recorded and 60 atoms evenly distributed in the blue area are selected to represent the vibrational properties of plane. Note that in the plane region, the *x*-direction and *y*-direction mode are in-plane modes and *z*-direction mode is an out-of-plane mode. In the fold region, only the *y*-direction mode is in-plane while the *x*-direction and *z*-direction mode are mixed modes, which contain both in-plane and out-of-plane modes.

with the increasing number of folds. In order to mimic experimental conditions (the inter-plane flux is usually negligible), the inter-plane heat flux is subtracted from the total heat flux.

The size dependence of revised resistivity on the characteristic sizes, $1/L$ and $1/L_{plane}$, are plotted in Fig. 4(a and b). It is shown that the thermal resistivity is still a linear function of the characteristic size, $1/L$ and $1/L_{plane}$. For folded graphene with L_{plane} = 6.75 nm, we obtain that η = 2.41, α = 0.20 from fitting the curves in Fig. 4(b). Therefore we can compare how the scattering time is affected by finite-size effects and phonon-folding scattering using $\frac{\tau_{finite}}{\tau_{folding}} = \frac{L_{plane}}{\alpha L}$. We find that when L is much larger than 33.75 nm, the finite-size effects dominate and folding scattering becomes negligible. When L is smaller than 33.75 nm, the finite-size effects are less significant than folding scattering.

We believe that the phonon-folding scattering regime is indeed phonon scattering at the entire region of fold induced by the folding structure. To further understand phonon-folding scattering, a phonon power spectrum of atoms in the plane and at the fold at room temperature is calculated. As shown in Fig. 5, the spectrum describes the power carried by phonon per unit frequency. In the MD simulations used to record the spectrum, there is no external thermostat applied.

A higher value of phonon spectral density (PSD) at a certain frequency f indicates that there are more phonons occupying states, whereas a zero value of PSD means that there are no

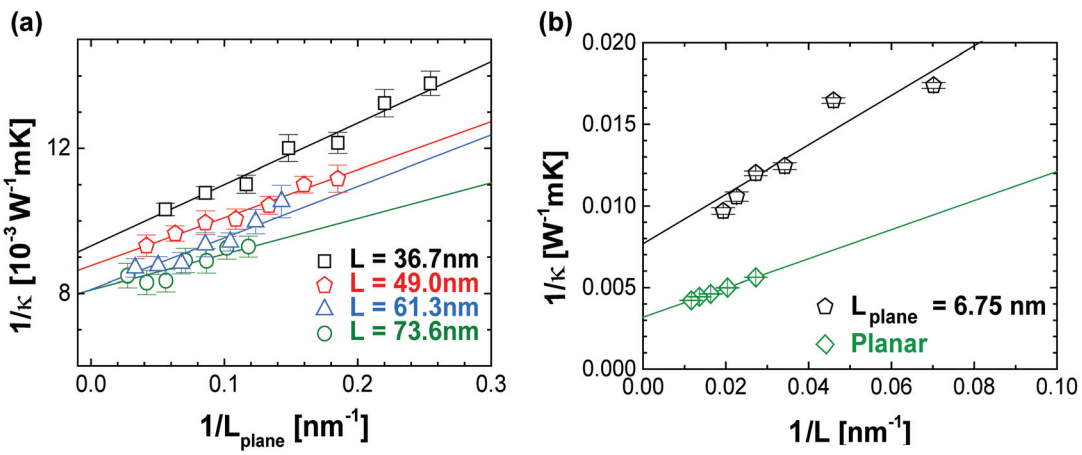

Fig. 4 (a) The dependence of revised resistivity of folded graphene on $1/L_{plane}$. (b) The dependence of revised resistivity on $1/L$ of folded and planar graphene.

such phonons existing. As is illustrated in Fig. 5, the power spectra of atoms in the plane are similar to graphene, where the in-plane/out-of-plane mode phonons are mainly distributed in high-frequency/low-frequency range.[33,34] However, we do not observe the same scenario for atoms in the power spectra of atoms at the fold. These spectra have significant differences from those of atoms in the plane because the cylindrical distribution of atoms leads to a mix of vibrations along different directions. The spectra at the fold are similar to those of nanotubes, of which the highest peak locates within the high-frequency range.[35,36] The mixed vibrations along different directions are also observed in the folded graphene nanoribbon.[15]

When phonons pass the fold, some phonons along the z direction need to change from the out-of-plane into a mixed mode, and change back to an out-of-plane mode after passing the folds. There are appreciable differences between the z-direction PSD of atoms at the fold and in the plane in low-frequency range (0–10 THz). The two peaks in power spectrum of atoms in the plane disappear when it comes to the fold, which means that low-frequency phonons are depressed. These mismatch behaviors of phonons will induce phonon scattering to redistribute the phonon energy to allow phonons to pass through the fold.

Finally, we would like to discuss the possibility of the experimental realization of the instantaneously adjustable thermal resistor. Our previous report[5] has shown that the number of folds/the length between two folds of large-area graphene can be easily controlled by changing the strain of the substrate, the shear modulus of the substrate, and the adhesion energy between the graphene and the substrate. This enables us to tune L_{plane} instantaneously while keeping L as a constant. Meanwhile, in this work, we have found that thermal resistivity calculated with or without subtracting inter-plane interactions both depend linearly on $1/L_{\mathrm{plane}}$. This ensures linear characteristics of thermal resistance. Based on these discussions, we believe that an instantaneously adjustable thermal resistor could be realized in the near future.

Conclusion

Similar to other nanostructures, the overall-length dependence of the thermal resistivity in folded graphene arises from the finite-size effects. Interestingly, the resistivity depends linearly on the length between two folds. The underlying physical mechanism is phonon-folding scattering, *i.e.* phonon scattering due to mode mismatch between the plane and fold, which has great impact on those phonons with MFP longer than the length between two folds.

Our results are of vital importance for building instantaneously adjustable thermal resistors. Since the number of folds/the length between two folds can be easily controlled by substrate deformation, the thermal resistance is directly determined by the strain executed on the substrate. Besides graphene, we believe that other 2D materials with a large phonon MFP can also be applied as adjustable thermal resistors by folding due to the applicability of phonon-folding scattering effect. The realization of the adjustable thermal resistor not only completes the spectrum of thermal analogs of electronics but leads to a brighter future with more possibilities for thermal devices based on adjustable thermal resistors.

Acknowledgements

This work was supported by the National Natural Science Foundation of China No. 51576067 (N. Y.) and No. 51572096 (J. Z.), and the National 1000 Talents Program of China tenable in HUST (J. Z.). We are grateful to Zelin Jin, Yingying Zhang, Dengke Ma and Shiqian Hu for useful discussions. The authors thank the National Supercomputing Center in Tianjin (NSCC-TJ) for providing assistance in computations.

References

1 N. Li, J. Ren, L. Wang, G. Zhang, P. Hänggi and B. Li, *Rev. Mod. Phys.*, 2012, **84**, 1045.
2 B. Li, L. Wang and G. Casati, *Phys. Rev. Lett.*, 2004, **93**, 184301.
3 B. Li, L. Wang and G. Casati, *Appl. Phys. Lett.*, 2006, **88**, 143501.
4 L. Wang and B. Li, *Phys. Rev. Lett.*, 2007, **99**, 177208.
5 J. Zang, S. Ryu, N. Pugno, Q. Wang, Q. Tu, M. J. Buehler and X. Zhao, *Nat. Mater.*, 2013, **12**, 321.
6 S. Anisimov and B. Kapeliovich, *Zh. Eksp. Teor. Fiz*, 1974, **66**, 375.
7 A. A. Balandin, S. Ghosh, W. Bao, I. Calizo, D. Teweldebrhan, F. Miao and C. N. Lau, *Nano Lett.*, 2008, **8**, 902.
8 S.-M. Lee, J.-H. Kim and J.-H. Ahn, *Mater. Today*, 2015, **18**, 336.
9 Y. Xie, Y. Chen, X. L. Wei and J. Zhong, *Phys. Rev. B: Condens. Matter*, 2012, **86**, 195426.
10 Z. Ni, Y. Wang, T. Yu, Y. You and Z. Shen, *Phys. Rev. B: Condens. Matter*, 2008, **77**, 235403.
11 E. Pop, V. Varshney and A. K. Roy, *MRS Bull.*, 2012, **37**, 1273.
12 N. Yang, X. Xu, G. Zhang and B. Li, *AIP Adv.*, 2012, **2**, 041410.
13 T. Ouyang, Y. Chen, Y. Xie, G. M. Stocks and J. Zhong, *Appl. Phys. Lett.*, 2011, **99**, 233101.
14 Y. Zheng, N. Wei, Z. Fan, L. Xu and Z. Huang, *Nanotechnology*, 2011, **22**, 405701.
15 N. Yang, X. Ni, J.-W. Jiang and B. Li, *Appl. Phys. Lett.*, 2012, **100**, 093107.
16 J. H. Seol, I. Jo, A. L. Moore, L. Lindsay, Z. H. Aitken, M. T. Pettes, X. Li, Z. Yao, R. Huang and D. Broido, *Science*, 2010, **328**, 213.
17 H. Casimir, *Physica*, 1938, **5**, 495.

18 P. K. Schelling, S. R. Phillpot and P. Keblinski, *Phys. Rev. B: Condens. Matter*, 2002, **65**, 144306.
19 N. Yang, G. Zhang and B. Li, *Nano Today*, 2010, **5**, 85.
20 K. E. Goodson and Y. S. Ju, *Annu. Rev. Mater. Sci.*, 1999, **29**, 261.
21 M. G. Holland, *Phys. Rev.*, 1963, **132**, 2461.
22 P. Klemens, *Solid State Phys.*, 1958, **7**, 1.
23 S. Nosé, *J. Chem. Phys.*, 1984, **81**, 511.
24 W. G. Hoover, *Phys. Rev. A*, 1985, **31**, 1695.
25 L. Yi, Y. Zhang, C. Wang and T. Chang, *J. Appl. Phys.*, 2014, **115**, 204307.
26 N. Yang, G. Zhang and B. Li, *Appl. Phys. Lett.*, 2008, **93**, 243111.
27 Y. Guo, N. Karasawa and W. Goddard, *Nature*, 1991, **351**, 464.
28 R. E. Tuzun, D. W. Noid, B. G. Sumpter and R. C. Merkle, *Nanotechnology*, 1996, **7**, 241.
29 N. Yang, S. Hu, D. Ma, T. Lu and B. Li, *Sci. Rep.*, 2015, **5**, 14878.
30 W. C. Swope, H. C. Andersen, P. H. Berens and K. R. Wilson, *J. Chem. Phys.*, 1982, **76**, 637.
31 S. Lepri, R. Livi and A. Politi, *Phys. Rep.*, 2003, **377**, 1.
32 O. Narayan and A. Young, *Phys. Rev. E: Stat. Phys., Plasmas, Fluids, Relat. Interdiscip. Top.*, 2009, **80**, 011107.
33 B. Mortazavi, M. Pötschke and G. Cuniberti, *Nanoscale*, 2014, **6**, 3344.
34 G. Sanders, A. Nugraha, K. Sato, J. Kim, J. Kono, R. Saito and C. Stanton, *J. Phys.: Condens. Matter*, 2013, **25**, 144201.
35 J. Shiomi and S. Maruyama, *Jpn. J. Appl. Phys.*, 2008, **47**, 2005.
36 V. Sokhan, D. Nicholson and N. Quirke, *J. Chem. Phys.*, 2000, **113**, 2007.